REPORT DOCUMENTATION PAGE

Form Approved
OMB No. 0704-0188

1. REPORT DATE (DD-MM-YYYY)	2. REPORT TYPE	3. DATES COVERED (From – To)
	Final Technical Report	1 April 2004 – 31 December 2006

4. TITLE AND SUBTITLE
High Temperature Liquid and Glass Precursors for Oxyphosphate Ceramic Composites

5a. CONTRACT NUMBER

5b. GRANT NUMBER
FA9550-04-1-0153

5c. PROGRAM ELEMENT NUMBER

6. AUTHOR(S)
Dr. William T. Petuskey

5d. PROJECT NUMBER

5e. TASK NUMBER

5f. WORK UNIT NUMBER

7. PERFORMING ORGANIZATION NAME(S) AND ADDRESS(ES)
Department of Chemistry & Biochemistry
Arizona State University
Box 871604
Tempe AZ 85287-1604

8. PERFORMING ORGANIZATION REPORT NUMBER

9. SPONSORING/MONITORING AGENCY NAME(S) AND ADDRESS(ES)
USAF/AFRL
AFOSR
875 North Randolph Street
Arlington VA 22203
Dr Joan Fuller/NA

10. SPONSOR/MONITOR'S ACRONYM(S)

AFRL-SR-AR-TR-07-0271

12. DISTRIBUTION AVAILABILITY STATEMENT

Distribution Statement A: Approved for public release. Distribution is unlimited.

13. SUPPLEMENTARY NOTES

14. ABSTRACT
The overall objective of this project has been explore the structure, dynamics and physical chemistry of rare earth aluminophosphosilicates (REAPS) glasses for the purpose of designing low temperature synthetic routes for fabricating high temperature, high fracture toughness ceramic-matrix-composites. The concept is based on a glass-ceramic approach that combines the densification of glass powders via viscous sintering followed by independent crystallization anneals. The challenge with REAPS glasses is to balance the design criteria for effective synthesis with the criteria of the composite applications. One objective was to find appropriate compositions that allowed sufficient range of temperatures to sinter glass powders above their glass transition temperatures to separately densify glass powders in their supercooled state with the hindrance of premature crystallization. In subsequent step, the densified glasses would be crystallized in a manner to produce microstructures of appropriate utility. The work undertaken has been to evaluate and understand the pertinent physical and chemical properties that are necessary for optimizing the chemistry that best meets both demands. Fortunately, we identified compositions that satisfy both sets of criteria with almost no compromise and the feasibility of the glass-ceramic approach for producing ceramic matrix nanocomposites was proven.

15. SUBJECT TERMS

16. SECURITY CLASSIFICATION OF:			17. LIMITATION OF ABSTRACT	18. NUMBER OF PAGES	19a. NAME OF RESPONSIBLE PERSON
a. REPORT	b. ABSTRACT	c. THIS PAGE	Unclassified	26	19b. TELEPONE NUMBER (*Include area code*)
Unclassified	Unclassified	Unclassified			(703)

Final Report

High Temperature Liquid and Glass Precursors for Oxyphosphate Ceramic Composites

A research project sponsored by the
Air Force Office of Sponsored Research

(AFOSR Grant Award #: F49550-04-0153)

For the research period 4/1/2004 to 12/31/2006

Submitted July 27, 2007

by

William T. Petuskey, Principal Investigator
Department of Chemistry & Biochemistry, and the School of Materials
Arizona State University
Box 871604; Tempe, AZ 85287-1604
480/965-5858; wpetuskey@asu.edu

Report Summary

The overall objective of this project has been explore the structure, dynamics and physical chemistry of rare earth aluminophosphosilicates (REAPS) glasses for the purpose of designing low temperature synthetic routes for fabricating high temperature, high fracture toughness ceramic-matrix-composites. The concept is based on a glass-ceramic approach that combines the densification of glass powders via viscous sintering followed by independent crystallization anneals. The challenge with REAPS glasses is to balance the design criteria for effective synthesis with the criteria of the composite applications. One objective was to find appropriate compositions that allowed sufficient range of temperatures to sinter glass powders above their glass transition temperatures to separately densify glass powders in their supercooled state with the hindrance of premature crystallization. In subsequent step, the densified glasses would be crystallized in a manner to produce microstructures of appropriate utility. The work undertaken has been to evaluate and understand the pertinent physical and chemical properties that are necessary for optimizing the chemistry that best meets both demands. Fortunately, we identified compositions that satisfy both sets of criteria with almost no compromise and the feasibility of the glass-ceramic approach for producing ceramic matrix nanocomposites was proven.

A summary of our research accomplishments were:

1. The liquidus temperatures for the binary Al_2O_3-$LaPO_4$ (alumina-monazite) and $Al_6Si_2O_{13}$-$LaPO_4$ (mullite-monazite) systems were determined and fitted to a thermodynamic model. We also mapped out the general liquidus surfaces for the ternary Al_2O_3- $Al_6Si_2O_{13}$-$LaPO_4$ system, although refinements are needed.

2. We determined the glass transition and crystallization temperatures for the $Al_6Si_2O_{13}$-$LaPO_4$ system as a function of composition and have identified the best compositions for exploring the glass-ceramic approach.

3. We explored the glass transition dynamics and identified a temperature regime of amorphous phase segregation (APS) that precedes the sequence of crystallization events.

4. We developed a model of the glass-forming network consisting of tetrahedral [AlO_4], [SiO_4], [PO_4] structural units and a set of rudimentary rules on their connectivity. This was based upon multinuclear one-dimensional MAS NMR of aluminum, silicon and phosphorus nuclei and selective two-dimensional, triple-quantum MAS NMR on aluminum and phosphorus.

5. We have explored the nucleation and growth dynamics of crystallization and have demonstrated that they can be manipulated to produce the composite microstructures desired.

6. We conducted a cursory viscous sintering study of glass powders demonstrating that sintering can be taken to near full density without incurring premature crystallization.

7. We developed a sol-gel method for producing alumina-aluminophosphosilicate glasses at low temperatures with a very low carbon residue. This chemistry might be adapted for large-scale production of REAPS glasses without resorting to quench melts.

Introduction

This project evolved from an early experiment conducted in the PI's laboratory that derived intriguing composite microstructures of $LaPO_4$ monazite and Al_2O_3 alumina from molten oxide solutions.[‡] Some of the resultant microstructures indicated that it would be possible to produce composite structures by directional solidification, with the capability to produce near ideal 1-D composite structures targeted by materials engineers for high fracture toughness ceramics. The typical traditional method of fabrication has been the densification of compacts of monazite-coated ceramic fiber bundles in polycrystalline ceramic matrices. On the other hand, we noted that the melting points of $LaPO_4$ and Al_2O_3 were known to be nearly identical (2072 and 2054 °C, respectively), and that the crystalline solids were immiscible in one another. Thus, this presented a classic case of a simple eutectic system from which a wide range of microstructures could be produced depending on the temporal and spatial control of a directional solidification process.

Figure 1 presents an example of highly attractive microstructure of Al_2O_3–$LaPO_4$ derived by directional solidification from the melt. This uniform microstructure consists of pure alumina grains (dark phase), about 10 μm in diameter, separated by a continuous boundary phase of La-monazite ($LaPO_4$) about 2 μm thick. The dimensions of this type of microstructure are comparable to what is being targeted by traditional ceramic fabrication methods[2].

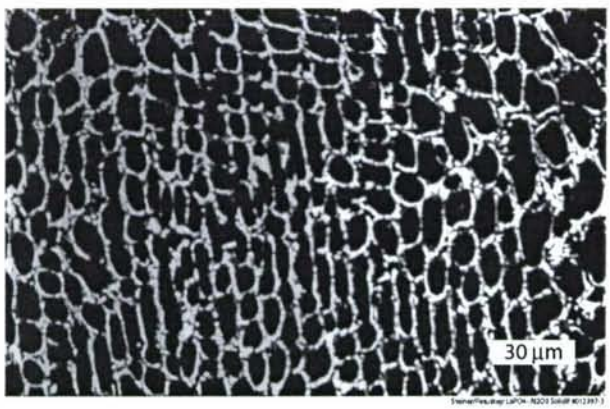

Fig. 1. Backscattered electron micrographs. ***Left****: a solidified microstructure from a* $75Al_2O_3$–$25LaPO_4$ *melt consisting of isolated corundum grains (dark) separated by a continuous boundary phase of La-monazite (bright phase).*[1]

Later, we realized that it was possible to produce homogenous glasses by rapidly quenching oxide-phosphate liquids. In effect, glasses are liquids whose structures are frozen in place due to quenching at such high rates that the kinetic limitations of molecular relaxation precluded the nucleation and growth of crystals. On the other hand, nucleation and growth from the glassy state has the potential of greater control, particularly in producing much finer composite structures than is possible from a melt supercooled directly from its equilibrium melting point. As such, very finely textured composites could therefore be formed which potentially

[‡] The microstructures shown in Fig. 1 were produced in those early experiments by Kimberly A. Steiner as a side project to her master's degree thesis work on the thermal expansion of layered structure perovskites. At the time, layered perovskites were being investigated as toughening agents for ceramic-matrix-composites (CMCs) (K. Steiner, M.S. thesis, Arizona State University, 1998) that were, in a sense, a competing technology to the monazite boundary phase CMCs.

would present properties of very high fracture toughness and pseudo-plasticity. The objective of this project was to demonstrate the feasibility of this essential point; that is, glasses could be viable precursors for nanostructured ceramic-matrix-composites.

The final point that was recognized early is that glass formation from such complex compositions, as those studied in this project would best be formed as fine powders from either rapidly quenching melts or by sol-gel processing. For most ceramic-matrix-composite (CMC) applications, large monolithic ceramic pieces are necessary. Therefore, greatest control would be attained where the glass powders were first densified into large bodies in the glassy state by viscous sintering. This would then be followed by crystallization from the glass. A good part of this project was devoted to understanding how the glass properties could be manipulated and engineered so that the glass transition, viscous sintering, and crystallization temperatures could be widely separated to accommodate independent densification and crystallization processes.

The following report summarizes the technical accomplishments of this project followed by additional details of activities to disseminate the information. This project funded the dissertation work of one doctoral student and one master degree students. It also provided opportunities for other students, both undergraduate and graduate, to conduct high level, high quality research that enriched their scientific training.

Program Acknowledgements

The principal investigator sincerely appreciates the financial support and encouragement of the Air Force Office of Scientific Research, supplied through the Directorate of Aerospace and Materials Sciences office on Ceramics and Nonmetallic Materials program (Dr. Joan Fuller, program manager).

Technical Results

The drive to develop high fracture toughness and oxidation resistant ceramic-matrix-composites (CMC's) has led to a number of innovations over the past decade. Highly notable has been the combination of lanthanum monazite ($LaPO_4$) with corundum (Al_2O_3), and the combination of lanthanum monazite with mullite ($3Al_2O_3{\cdot}2SiO_2$), in fiber-based CMC's and in thermal barrier coatings[3-6]. Fracture toughening is attributed to poor interfacial bonding at phase boundaries and to the tendency of monazite to exhibit some form of plastic deformation involving dislocation slip, particularly at high temperatures. Several approaches involving accepted ceramic methodologies have been taken in fabricating these composites. Each has their advantages, and each has benefited from the devotion of considerable ingenuity, effort and expertise. However, the application of oxide-phosphate composites is still in a very early stage, due to technical limitations of each method. We were interested in exploring an alternative approach that uses glass powders as precursors to ceramic composites that may be formed as either a monolithic ceramic body or as a component integrated into a functional material assemblage. As will be shown, the glass compositions and crystallization dynamics can be engineered to optimally producing microstructures of load-bearing ceramic components (e.g., mullite or alumina) in a continuous boundary layer matrix of lanthanum monazite. The purpose of this project has been to survey the glass properties to identify what ranges are optimal for composite manufacture from glasses.

The glass-ceramic approach is an old concept that has been successfully applied for producing a wide range of functional ceramic materials. Its applications range from dinner-wear to high performance electronic components. The concept combines the advantages of easier forming capabilities of the glass with the superior physical properties of the crystalline solid after it has been converted. Overall, fabrication follows a lower temperature pathway than would have been possible via other prevailing technologies.

In our particular case of Rare Earth AluminoPhosphoSilicates (REAPS), the targeted concept has been to identify compositions that would allow the independent steps of densifying glass powders via viscous sintering and then converting the glass into composites via controlled crystallization anneals. Amorphous substances often have greater densification rates than their crystalline counterparts because of the markedly different mass transport mechanisms. At the same time, crystallization from a glass is generally carried out at much lower temperatures than that required for solidification from a melt. For this reason, it is possible to generate finer microstructures from a glass and thereby manipulate mechanical and other physical properties to an extreme of what would be desired from a composite.

As mentioned in the introduction, we were intrigued with the fact that both alumina and lanthanum phosphate monazite possessed nearly the same melting points, i.e., 2054 and 2072°C, respectively, and yet were immiscible in the solid state. This led us to think that composites could be grown from the melt. We quickly learned that it was possible to easily form Al_2O_3-$AlPO_4$ glasses and, somewhat less easily, Al_2O_3-$LaPO_4$ glasses. We expanded our study from the La_2O_3-Al_2O_3-P_2O_5 system to the La_2O_3-Al_2O_3-P_2O_5-SiO_2 system for practical reasons that will be described later. Our focus has been on phosphorous-poor compositions [$P/(La + Al + P + Si) < 0.5$] because of their much

greater thermal stability than phosphorous-rich compositions and their applicability to high temperature CMC's.

There are two essential features of the glass-ceramic approach that need to be satisfied. One is that a glass can be made of the composition of the final crystalline ceramic. While glasses can be made of almost any substance, the practicality of quenching a liquid depends on the limitations of quench rates relative to the structural relaxation rates exhibited by the liquid/glass. In some cases, clever chemical synthetic routes can by-pass the need for quenching melts. The implications are that glasses must be readily and reliably synthesized in order to be of value for a glass-ceramic approach as is proposed here. We show in the following that REAPS glasses can be by synthesized by both melt quenching and sol gel synthesis (with little residual carbon).

The second essential feature is the need of a significant spread between the glass transition and crystallization temperatures. Densification of a glass via viscous sintering is most efficient without any interference due to coincident crystallization. This implies that there must be significant barriers to nucleation and growth of crystals at the sintering or forming temperature. Therefore, we seek glasses that are complex in the constitution of their network, thus imposing a very large entropic penalty in allowing crystals to nucleate.

The following sections describe the results of this project on the fundamental characteristics of REAPS glasses and melts. It addresses why we think these glasses are suitable for the glass-ceramic approach. That is to say, that REAPS glasses possess the important characteristics that are necessary for successfully applying them as precursors for ceramic composites. Good sinterability and microstructure control are demonstrated, indicating that a low temperature glass-ceramic route is plausible. Fortuitously, the optimal glass compositions from a mechanistic view correspond to the compositions that we would consider desirable for ceramic matrix composites. As such, we are targeting glass compositions that are around 60 mol% mullite and 40 vol % monazite (i.e., 78 vol % $Al_6Si_2O_{13}$ – 22 vol% $LaPO_4$).

Phase chemistry of the La_2O_3-Al_2O_3-P_2O_5-SiO_2 system. The phase chemistry of the La_2O_3-Al_2O_3-P_2O_5-SiO_2 quaternary system was investigated for compositions of interest for glass formation and composite fabrication. The compatibility relationships between solids and the liquidus surfaces were determined as a function of composition. We actively investigated the La_2O_3-Al_2O_3-P_2O_5 and the $LaPO_4$-Al_2O_3-SiO_2 ternary sections of the quaternary system. The sub-solidus studies were conducted on samples annealed at high temperatures combined with room temperature analyses by powder x-ray diffraction analysis (XRD) and electron probe microanalysis (EPMA).

Figure 2 (left) exhibits the compatibility relationships experimentally determined for the La_2O_3-Al_2O_3-P_2O_5 system within the context of the quaternary axes. Generally, lanthanum phosphate monazite, $LaPO_4$, is compatible with most solids in the phosphorous-poor compositions of the system. This includes alumina itself, the magnetoplumbite phase $LaAl_{11}O_{18}$, $LaAlO_3$ and La_5AlO_9. It is also compatible with crystalline $AlPO_4$ (berlinite). Figure 2 (right) shows the $LaPO_4$-Al_2O_3-SiO_2 ternary section. This is considered to be a true ternary system since $LaPO_4$ monazite is compatible with alumina, crystalline mullite, $Al_6Si_2O_{13}$, and crystalline silica (cristobalite

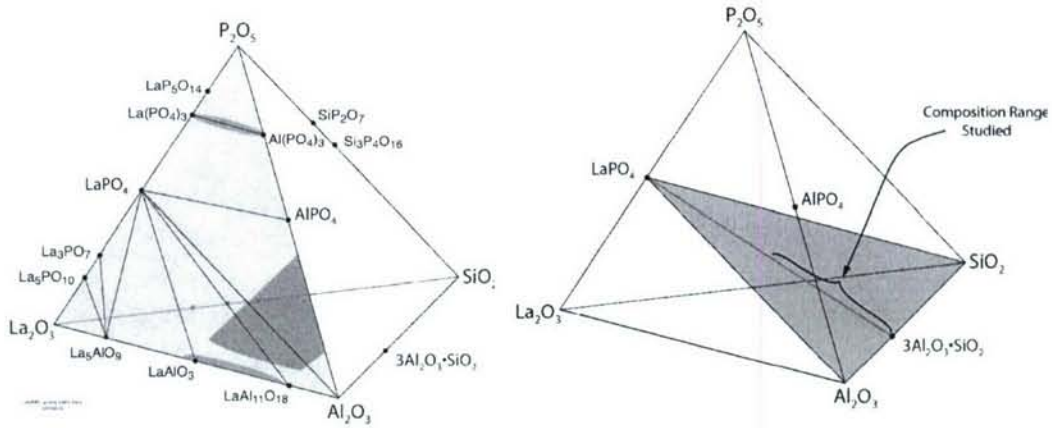

Fig. 2. **Left**: Phase compatibility relationships of the La_2O_3-Al_2O_3-P_2O_5 ternary system are displayed on the front face of the La_2O_3-Al_2O_3-P_2O_5-SiO_2 quaternary axes. Red shading indicates the extent of glass formation studied by this project. Dark blue shading indicates glass forming regions identified by other investigations[7,10]. Right: Crystalline phase compatibility within the $LaPO_4$-Al_2O_3-SiO_2 section of the system. Phase compatibility between mullite, $Al_6Si_2O_{13}$, and lanthanum monazite, $LaPO_4$, is shownby the red Alkemade line. The range of compositions for glasses studied for most of this project is indicated along this join. Relative compositions are to scale and expressed in terms of cation fraction [X/(La + Al + P + Si)].

at these temperatures). It is interesting to note here that when aluminum phosphate is included, the quaternary section $LaPO_4$-$AlPO_4$-Al_2O_3-SiO_2 represents does not exhibit any complex phases within this composition range. This is the composition range of greatest interest to us for glass formation and composite formation.

The shading in Fig. 2 (left) indicates the composition ranges for which glasses have been discovered and studied. Our initial interest focused on the larger area outlined near the alumina rich region of the monazite-alumina join and bridging towards the Al_2O_3-$AlPO_4$ join. Other glass forming compositions include the $La(PO_4)_3$-$Al(PO_4)$ join, which have been studied extensively for their potential applications as laser hosts and other optical materials[7-9]. Alumina-lanthana glasses, without phosphates, have been the subject of considerable interest to a group at 3M corporation, for much the same reasons that we have stated as our justification for this study[10]. That is to say, the synthesis of high temperature, high quality composites may be achievable via the low temperature route of viscous sintering in the glassy state and subsequent by crystallization anneals.

We measured the liquidus surfaces for selected regions of the quaternary system. This was done using a high temperature microscope designed for this project that consisted of optical components with long working distances, a CCD camera and iridium wire furnace. Temperature calibrations were made using substances of reported melting points. The two diagrams shown in Fig. 3 (left) illustrate simple eutectic melting relationships for the binary systems Al_2O_3-$LaPO_4$ and $Al_6Si_2O_{13}$-$LaPO_4$. The essential difference in these two diagrams relates to the slopes of the liquidi. In the alumina-

monazite diagram, the slopes are rather steep and straight, indicating that the thermodynamics of the liquid may be deceptively simple. As will be discussed later, glass formation is rather difficult, requiring rather high quench rates. On the other hand, the mullite-monazite diagram exhibits a relatively flat liquidus in equilibrium with mullite. Such features are commonly seen for chemical systems on the verge of forming a miscibility gap (e.g., alkaline earth-silica binary systems[11]). Corresponding to this, we have found glass formation to be relatively easy, which is fortunate since this is the composition range of greatest interest for mullite-monazite composites.

The liquidus surfaces for the mullite-monazite-alumina ternary system are mapped out in Fig. 3 (right). This represents almost the full range of glass compositions that is of prime interest to us. The contours were calculated from a liquid thermodynamic model derived and fitted to the experimental data collected for two binary systems and the data indicated in the ternary diagram. We also used information taken from the literature for the mullite–alumina system. Unlike the Al_2O_3-$LaPO_4$ and $Al_6Si_2O_{13}$-$LaPO_4$ systems, which are both binary eutectics, the $Al_6Si_2O_{13}$- Al_2O_3 diagram is more complex. The composition of mullite phase, in equilibrium with the monazite and mullite phases, shifts from right to left as temperature is decreased. It emphasizes that mullite's own composition invariably changes with temperature when it is in equilibrium with a liquid. At first glance, the ternary diagram appears to be that of a ternary eutectic, where the eutectic trace follows the curved line at the mullite corner of the diagram. Instead, this line denotes not only the equilibrium composition of liquid, but it also infers the composition of the mullite phase, as well. This is determined be extending a line from

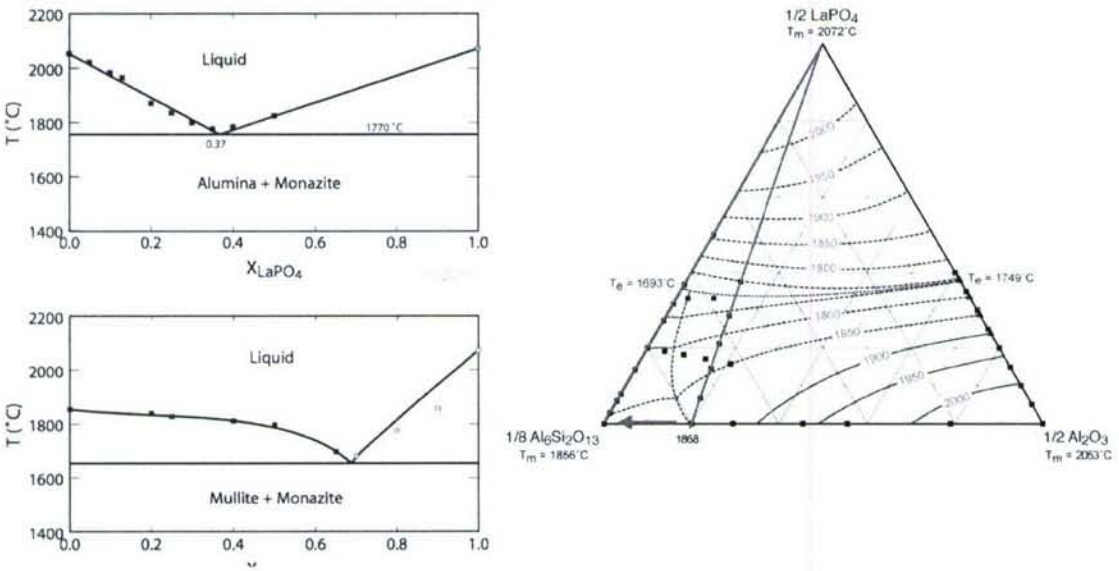

Fig. 3. Liquidus temperatures measured using high temperature microscope. Lines are calculated from thermodynamic fits. **Top left**: Al_2O_3-$LaPO_4$ system. **Bottom left**: $Al_6Si_2O_{13}$ (mullite) – $LaPO_4$ (monazite) system. Right: Ternary system mullite–monazite–alumina.

the $LaPO_4$ vertex through the liquid eutectic line for the composition-temperature of interest to the mullite-alumina join. As such, the compatibility line is seen to shift from right to left. The ternary eutectic for the system lies quite close to the mullite–monazite join.

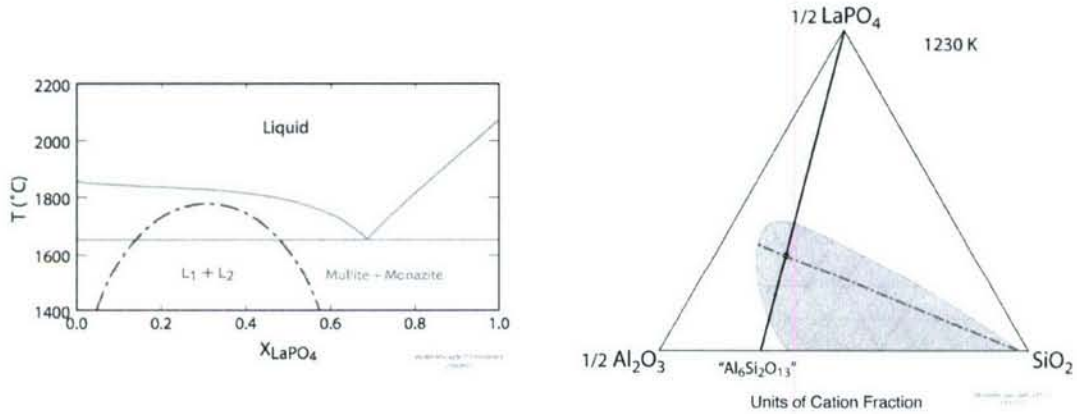

Fig. 4. ***Left****: Schematic of the miscibility gap in the metastable liquid of the $Al_6Si_2O_{13}$–$LaPO_4$ system. While implied by the shallow liquidus for mullite, experimental results strongly indicates its existence.* ***Right****: Schematic of a miscibility gap in ternary metastable liquid for the $Al_6Si_2O_{13}$–$LaPO_4Al_2O_3$ system at about 957°C. The dashed line connects two glass compositions experimentally observed that cuts across the compatibility line connecting monazite, $LaPO_4$ and mullite, $Al_6Si_2O_{13}$. The compositions indicated for the miscibility gap in the mullite–alumina system were extrapolated from the literature.*

The Al_2O_3–SiO_2 system exhibits a metastable miscibility gap[12]. Consequently, it should not be surprising that one should appear in the $LaPO_4$–$Al_6Si_2O_{13}$–Al_2O_3. Evidence is shown later in this discussion, however, Fig. 4 shows schematically the miscibility gap for the $LaPO_4$–$Al_6Si_2O_{13}$ binary and $LaPO_4$–$Al_6Si_2O_{13}$–Al_2O_3 ternary diagrams. That for the ternary system is partially based on experimental compositions determined from work on the mullite-alumina system and our own work on the monazite–mullite binary system. At least on the ternary plane of this system and in the vicinity of the glass transition temperatures (850 to 950°C), the miscibility gap is quite extensive for the supercooled liquids. This has significant ramifications when considering the early events of nucleation and growth from the glass.

<u>*Glass formation and relaxation dynamics*</u>. Our exploration of the glass forming capabilities began with the La_2O_3-Al_2O_3-P_2O_5 system, as represented by the front face of the quaternary system shown in Fig. 2 (left). Other investigations have focused on the low-melting glass behavior of the phosphate-rich region between $La(PO_4)_3$ and $Al(PO_4)_3$[7,8], and on the phosphorous-free, alumina-rich compositions along the La_2O_3-Al_2O_3 join[10]. The latter case has been of interest for a number of reasons but notably for its polyamorphic behavior, like many rare earth aluminates. Such glasses have a tendency to decompose via a spinodal mechanism into two glasses of the same composition but of different densities[13-17].

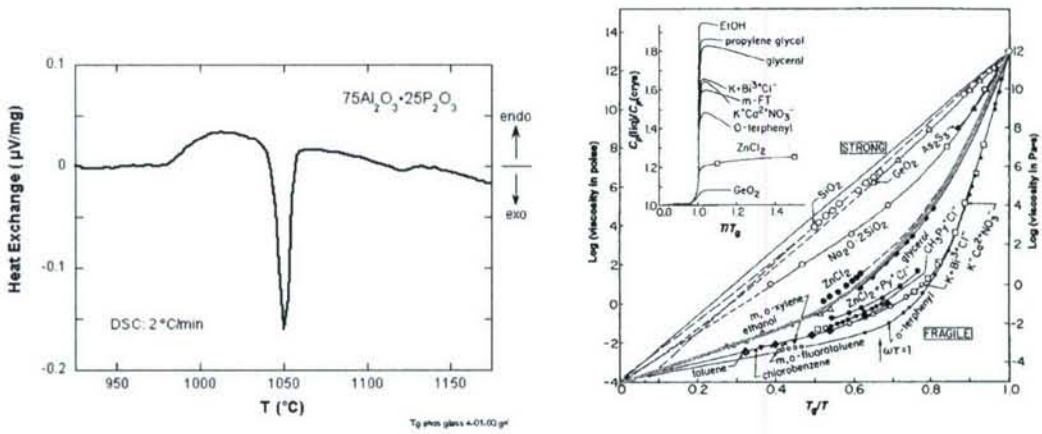

C. A. Angell, Science, 267, 1924-1935 (1995)

Fig. 5. ***Left****: DSC trace of through the glass transition and crystallization temperatures for 50:50 $AlPO_4$:Al_2O_3 ($75Al_2O_3$•$25P_2O_5$) glass. The glass transition occurs at about 958°C.* ***Right****: Using the DSC data for glass transition and enthalpy rise, the viscosities were estimated as a function of temperature using the procedure of Moynihan[10]. The red curve superimposed on the fragility plot of Angell[18], indicates that this glass is rather fragile. This is typical for REAPS glasses.*

Our early research demonstrated glass formation capabilities along the Al_2O_3–$AlPO_4$ and Al_2O_3–$LaPO_4$ compositional joins. Glasses were made by thermally quenching melts generated using a xenon lamp imaging furnace where molten drops between 1-2 mm diameter were quenched in water. The glass transition temperatures, T_g, were generally quite high, even for inorganic glasses. For example, glassy Al_2O_3•$AlPO_4$ exhibited a relatively strong enthalpic glass transitions at T_g = 978°C, as is shown in Fig. 5 (left). An interesting feature of these glasses is that they are behaviorally "fragile". That is to say that structural relaxation as measured by viscosity is very non-Arrhenian in nature. Figure 5 (right) shows the viscosity of this glass as function of temperature superimposed on top of the master plot for all glasses that was introduced by Angell[18]. Unlike SiO_2, which is classified as a strong glass, these glasses exhibit most of their structural relaxation close to the glass transition temperature. This could be deduced by the rather large endothermic rise just above T_g indicating significant heat absorption as the structure adjusts.

The ability to make glasses along the Al_2O_3–$LaPO_4$ join was more challenging. The quench rate possible using our imaging furnace synthetic scheme (with a quench rate of about 500 to 1000 °C/sec) was insufficient to produce pure homogeneous glasses. The higher quench rates accessible from a hammer quench apparatus (about 3000 to 6000 °C/sec) did produce glasses more reliably, although these were not 100% homogeneous. The existence of minor precipitates of a lanthanum phosphate complicated and biased our fundamental studies of the glass relaxation and crystallization behavior Consequently, we changed our focus to glasses containing SiO_2, but still limited our attention to compositions that would yield relatively high melting point composite structures.

Figure 2 (right) exhibits the $LaPO_4$-Al_2O_3-SiO_2 ternary plane of the quaternary system. The binary join between monazite ($LaPO_4$) and mullite ($Al_6Si_2O_{13}$) represents a true binary in that both solids are compatible with one another and do not react except to form a liquid phase at high temperature. The diagram indicates the composition range that we have given most of our attention. This corresponds to the liquidus shown in the Fig. 2 (bottom left) that is shallowly sloped. These compositions, between 25 to 85% mullite (75 to 15% monazite), were the most appropriate for glass formation.

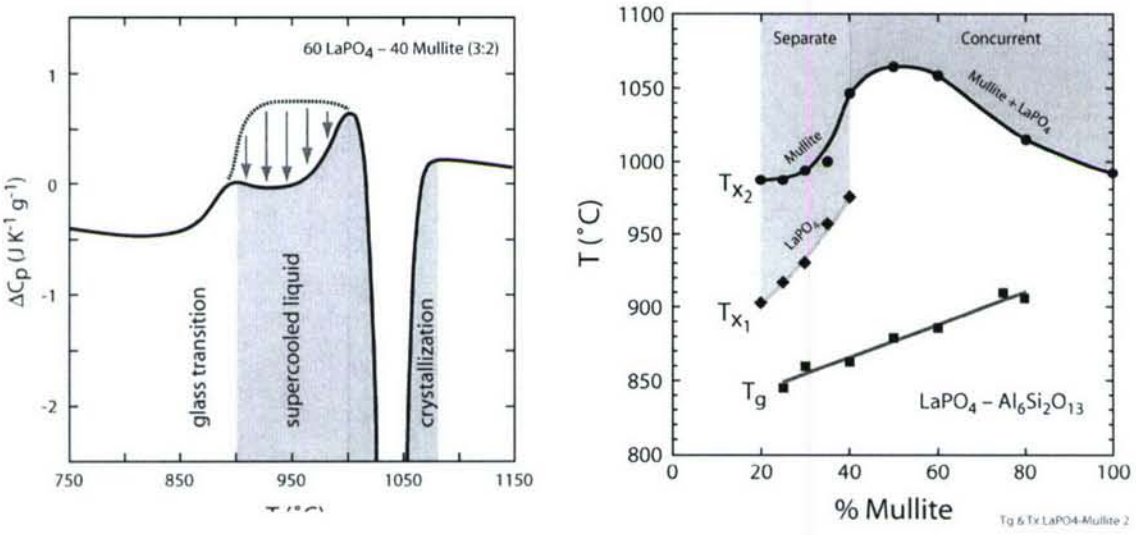

Fig. 6. ***Left****: Thermal signature of a REAPS glass obtained by differential scanning calorimetry.* ***Right****: Glass transition, T , and crystallization , T_x, temperatures as a function of composition.*

The dynamical behavior of the $Al_6Si_2O_{13}$–$LaPO_4$ (mullite–La-monazite) glasses exhibit rather complex behavior. The DSC thermal signature of a 40M60L glass shown in Fig. 6(left) is typical of intermediate compositions where the network is known to consist of coordination tetrahedra of all three cations Al, Si and P. Upon heating, the glass transition precedes all other reaction events and appears as the first endothermic rise. As such, T_g was found to increase with the content of mullite, ranging from about 848 to 920°C for the compositions tested. A second endothermic rise is noted within the region denoted as supercooled liquid. This is related to amorphous phase segregation. The large exothermic peak marks crystallization.

Figure 6(right) summarizes the glass transition and crystallization temperatures as a function of composition. At low mullite compositions, two crystallization events are observed – one corresponding to lanthanum phosphate precipitation at low temperatures, and a second higher temperature peak corresponding to mullite. At intermediate to high mullite contents, only one crystallization peak is observed which corresponds to the simultaneous, and cooperative crystallization of lanthanum phosphate and mullite. The crystallization temperature, T_x, is mapped out as a function of composition on the same plot. It reaches a maximum at about 50% mullite – 50% monazite (50M50L).

The maximum in the crystallization temperature marks the compositions that would be best for developing glass ceramic precursors for reasons of ease in handling glass powders. For the compositions between 40 and 60% mullite, there is nearly a 200°C difference between T_g and T_x. This implies that it would be possible to work with glass powders, taking advantage of their flow characteristics without much concern over the interference of crystallization. Fortunately, the corresponding proportions of crystalline monazite and mullite are about 60 to 80 volume % mullite and 40 to 20 volume % monazite. This is very attractive for CMC designs.

For these compositions, the thermal signature between T_g and T_x suggests greater complexity in the relaxation processes than is usually seen in simpler glasses. For all glasses, it is expected that the glass transition would span over a range of temperatures, T_g to T_g'[19,20]. The DSC trace for a simple, single component glass would be expected to level off above T_g' up to the crystallization temperature. However, in the case of REAPS glasses, the DSC signal initially levels off and then takes another pronounced endothermic rise. Examination of materials annealed between T_g and T_x by high resolution electron microscopy and electron energy loss spectroscopy reveals that the supercooled liquid separate into two amorphous phases of different compositions, and that the complexity of the DSC curve may be related to heats of these processes.

Pre-crystallization Reactions in the Amorphous Phase.

Previous discussion of the DSC thermal signature in Fig. 6(left) already pointed out the anomaly of an endothermic rise in addition to the glass transition and just below the onset of crystallization. This may be explained in two ways, both related to some aspect of amorphous phase segregation. The first indication of phase segregation in the supercooled liquid is shown in Fig. 7, which shows a TEM micrograph of a glass chard annealed at 960°C which is in the middle of the supercooled, metastable liquid domain but below its crystallization temperature. Inset to that photograph is a composite image of the elemental mapping by electron energy loss spectroscopy (EELS). This shard clearly shows two different compositions. Electron diffraction confirms that they are both amorphous. The right lobe of the chard is nearly pure amorphous silica as indicated by in blue. The left lobe is a glass rich in lanthanum aluminate phosphate. This dissociation is thought to be related to what already has been observed in the dissociation of pure mullite glass into alumina and silica-rich phases. The miscibility gap in the ternary system is shown in Figure 4 (right). Dissociation of the amorphous phase is shown by the red line. The ends of this line correspond to the

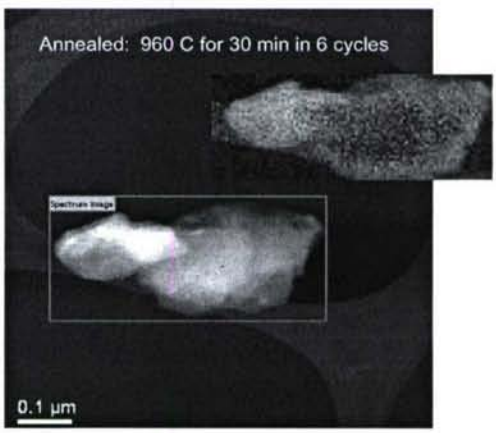

Fig. 7. TEM image and EELS compositional map (inset) of REAPS glass ($Al_6Si_2O_{13}$•$LaPO_4$) annealed midway between glass transition and crystallization temperatures revealing amorphous compositional segregation. Red-yellow-green particle is lanthanum phosphate rich glass; blue-aqua particle is aluminosilicate rich glass.[1]

compositions measured by EELS, which do not align with the compositions of the Alkemade line that connects the compositions of mullite and monazite and represents the most stable equilibrium. It is evident that amorphous phase segregation deviate from the compositions of the most stable equilibria. In the events leading to crystallization, silica is the first component to separate out.

This can be explained on the basis of the thermodynamics of metastable Al_2O_3-SiO_2 liquids. A thermodynamic analysis[12] of mullite itself indicates that the enthalpy of demixing is negative. Thus, for the reaction

$$Al_6Si_2O_{13} \xrightarrow{960^{\circ}C} 3Al_2O_3 + 2SiO_2 \quad \Delta H^{\circ}_{rxn} = -18.6\ kJ$$

The enthalpy of demixing is exothermic. This is based upon crystalline mullite decomposing to the corundum and quartz phases. By analogy, it may be presumed in the case of REAPS glasses that the precipitation of silica glass is also exothermic. This would appear as an exothermic reaction superimposed on the glass transition and the supercooled liquid regimes. Figure 6(left) schematically traces out a dashed line that suggests how the thermal signature might have appeared had the glass remained homogeneous. The endothermic rise just before crystallization might therefore be related to a second reaction of alumina exsolving from the glass and recombine with the silica to form a nascent amorphous embryo for mullite crystallization.

A schematic interpretation of the miscibility gap in the Al_2O_3-SiO_2-$LaPO_4$ ternary is shown as the shaded region in Fig. 4(right). This appears as an extension from the miscibility gap in the silica-alumina binary. Whereas crystalline mullite and monazite are thermodynamically compatible with one another, segregation within the glass moves off of the compatibility line. The dashed red line connects nearly pure glassy silica with the glassy lanthanum aluminate phosphate and shows that the thermodynamic rules of the glass are counter to those followed by the crystalline phases.

The nature of these glass reactions need to be examined more carefully since there are many different uncertainties and unexplained aspects. For instance, DSC of glasses previously annealed as supercooled liquids do not show the second endothermic rise. This might be explained by the alumina-silica recombination being pushed to higher temperatures where it cannot be easily seen in the very exothermic crystallization peak. However, this is only speculation that needs clarification.

The observation of compositional segregation in the supercooled liquid is intriguing for ceramic composite production because it suggests that it is an added variable to control the nucleation-growth and microstructure of the final composite. One of the aims of this project has been to understand the nature of amorphous phase segregation and how it influences high temperature crystallization. Compositional segregation within the glass will undoubtedly affect the nucleation and growth of the crystalline phases at higher temperatures. A future goal will be to carefully examine this phenomenon and seek out methods for manipulating the segregation as a means of controlling nucleation, growth and directionality of the crystalline microstructure.

The DSC thermal signature in Fig. 6 (left) can therefore be explained by a mild exothermic segregation event superimposed on the thermal trace between T_g and T_x. Figure 6 schematically illustrates this point by the difference of the dashed line and the

true DSC trace. If this reaction did not occur, it would have been expected that the endothermic rise would plateau at a higher temperature as indicated by the dashed line. However, the relaxation mobility is fast enough to allow components to diffuse and segregate, thereby releasing heat during the process, and forcing the trace in an exothermic direction (red arrows). Despite these changes, crystallization still does not occur without much longer annealing. In the next section the determination of time-temperature-transformation (TTT) diagrams are discussed.

The observation of compositional segregation in the supercooled liquid is intriguing for CMC production because it suggests that this could be an added variable to control the nucleation-growth and microstructure of the final composite. One recommendation for future research is to understand the nature of amorphous phase segregation and how it influences high temperature crystallization. Proper manipulation of amorphous phase segregation and other early events of nucleation implies considerable control of crystalline microstructures, whether they be random or directional.

Glass-structure of phosphorous poor compositions. We studied the structure of the quenched melt glasses of the mullite-monazite system as function of composition and as a function of temperature. The purpose was to gain insight into what is needed in forming glasses that are stable at higher temperatures and what features tend to suppress crystallization. Our work provided a basis for rationalizing the thermodynamic driving forces for forming liquids of complex networks and in explaining the driving forces for amorphous phase separation and crystallization. We relied most heavily on multinuclear MAS-NMR where the nuclei ^{27}Al, ^{31}P and ^{29}Si are routinely probed. Examples of ^{27}Al spectra of alumina-aluminum phosphate glasses are shown in Fig. 8, illustrating the kind of features that have been useful for interpreting structural trends.

In Fig. 8 (upper left), a series of one-dimensional ^{27}Al MAS NMR spectra are shown as a function of compositions along the mullite – $LaPO_4$ compositional axis. Here compositions are expressed in terms of mole percent $Al_6Si_2O_{13}$ and $LaPO_4$. The one dimensional spectra show what appears to be three maxima. At first it is tempting to suggest that these correspond to tetrahedral, pentahedral and octahedral coordinated aluminum. However, the two- dimensional ^{27}Al MAS NMR in Fig. 8 (upper right) reveals a different interpretation. The summation of the peak intensities along the horizontal MAS axis would be equivalent to the spectra seen on the left. However, vertical delineation along the isotropic axis reveals that there are really only two coordination states, one that is dominant. The large and broad peak centered about 45 ppm corresponds to tetrahedrally coordinated aluminum. Its breadth indicates a broad range of environments in the second and higher coordination spheres. The smaller peak centered at about 25 ppm corresponds to pentahedrally coordinated aluminum. Its presence is much smaller than the tetrahedral coordination, which is most dominant. It is interesting to note that octahedrally coordinated aluminum is not seen at all as is the case for pure mullite glasses and other glasses of high aluminum contents. This has implications about the role of aluminum in stabilizing the glass network.

Figure 8 (lower left) exhibits a MAS NMR spectrum of ^{29}Si. By-and-large, silicon is tetrahedrally coordinated to oxygen in these glass networks. The differences lie in the second and higher order coordination spheres. In evaluating the this spectrum the sharp peak located at -50 ppm can be disregarded since it represents the silicon located in

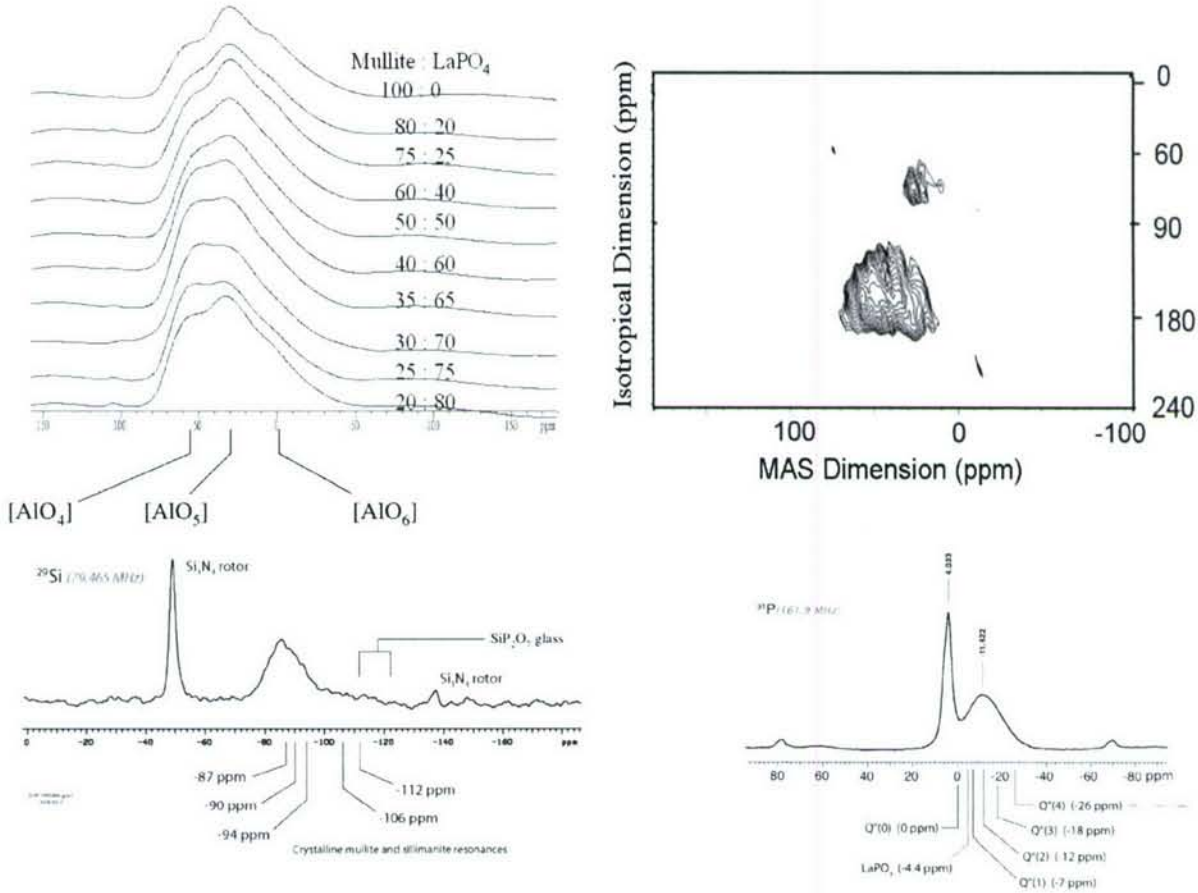

Fig. 8. Multinuclear MAS-NMR spectra of REAPS glasses (as quenched). Upper left: One dimensional ^{27}Al NMR of mullite–$LaPO_4$ glasses at difference compositions. Upper right: Two dimensional, 3Q ^{27}Al NMR on $30Al_6Si_2O_{13}$–$LaPO_4$ (30M70L) glass. Lower Left: One dimensional ^{29}Si MAS NMR spectrum of 30M70L glass. Lower Right: One dimensional ^{31}P MAS NMR spectrum of 30M70L glass.

the silicon nitride rotor that held the samples. The broad peak centered at about -85 ppm is in the same range as has been reported for pure mullite glasses. This suggests that the extended coordination spheres of silicon would be representative of an aluminosilicate glass. However, it is apparent from the aluminum NMR that this would be principally a glass network that was constructed of tetrahedral aluminum and silicon with little else of high order aluminums.

The ^{31}P MAS NMR is shown in Fig. 8 (lower right). Like silicon, phosphorus resides in four-fold coordination with oxygen where the differences in chemical shift are attributed to higher order coordination. A comparison to the chemical shifts in aluminum phosphate crystal and glass suggests that each tetrahedral phosphorus is connected to the extended glass network through an average of two oxygen linkages. This implies that

phosphorus itself resides on the edge of domains of the tetrahedral networks and lies close to the network modifying cations, namely, lanthanum in this case.

In combining the interpretations of these NMR studies, our understanding of the glass structure, thus far, indicates that tetrahedrally coordinated aluminum [AlO_4], phosphorous [PO_4] and silicon [SiO_4] all participate in forming the glass network. In keeping with the general understanding of many inorganic glass structures, these tetrahedra are corner linked and extend throughout the glass in all directions. However, the coordination state of aluminum is more complex. NMR also shows the presence of five-fold [AlO_5] and almost no six-fold [AlO_6] coordinated species, the concentrations of which depend on the overall composition and thermal history. Investigations on phosphate-rich rare earth aluminates[7-9,21], on amorphous mullite[22,23], and on high temperature alumina-monazite liquids[24] have already shown that tetrahedral aluminum is favored in the liquid state compared to the crystalline state where octahedral is most favored. A significant fraction of pentahedral aluminum is found in the confused structures of glasses and a few crystalline solids like mullite itself.

Figure 9 summarizes the general trends in aluminum coordination in a glass network's of the La_2O_3–Al_2O_3–P_2O_5–SiO_2 system as deduced from this study and other studies reported in the literature[25-31]. It is evident that aluminum has a central role in stabilizing the glass structure when it is in the right environments. Aluminum is actually promoted into tetrahedral coordination when it is needed to separate [SiO_4] and [PO_4] tetrahedra in the glass network. This is because of the relatively high oxidation states of Si^{4+} and P^{5+}, relative to Al^{3+}, and the need for the system to reduce electrostatic repulsions between cations. This means that Al–O–P and Al–O-Si linkages are favored over P–O–P, P–O–Si and, perhaps even, Si–O–Si linkages.

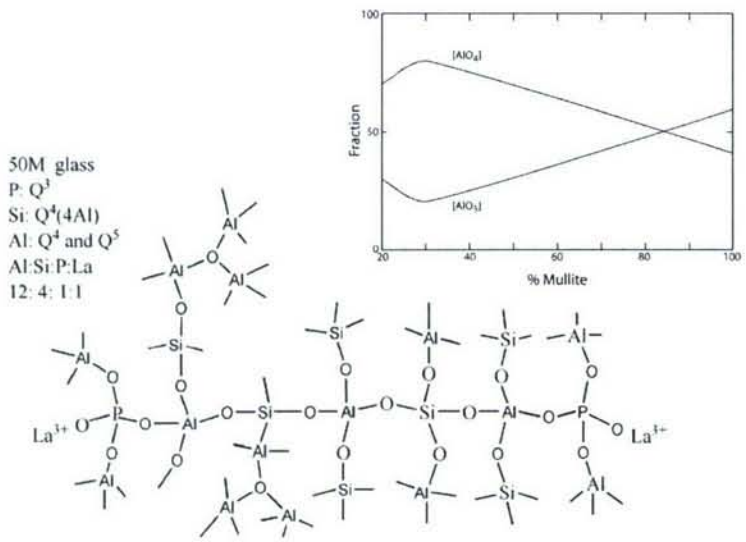

Fig. 9. Schematics of the important structural features implied from the NMR studies of REAPS glasses. The connectivity pattern in the tetrahedral network suggests regions of aluminosilicate glass bound by phosphorus and, possibly, pentahedral aluminum. Lanthanum ions reside close to the phosphorous.

The inset in Fig. 9 approximates the relative percentages of aluminum coordinations in REAPS glasses as a function of mullite content. Tetrahedral aluminum is dominant between 20 and 80% mullite. It is between 80 and 100% mullite where

pentahedral aluminum seems to make up a significant, and even dominant, fraction of the structure. In pure mullite glasses, it is known that significant fractions of the glass are actually five-fold aluminum. At the same time, notable fractions are six-fold, coordinated aluminum. It is interesting to note that we were not able to produce homogeneous glasses in this composition range. We always obtained a significant volume of crystalline phases, suggesting that the glass structure was too unstable to be quenched.

Considering this role for aluminum, it should not be surprising why the optimal composition for sintering and crystallization studies centers around the general composition of 60% mullite – 40% La-monazite. In the liquid and glassy states, aluminum mixes intimately and homogeneously in the glass network with silicon and phosphorous. However, upon crystallization, it segregates with silicon and dissociates completely from phosphorus. This suggests that demixing in this matter will set up a barrier to crystallization. In turn, this forces crystallization to occur at higher temperatures and thereby increase the spread between T_g and T_x.

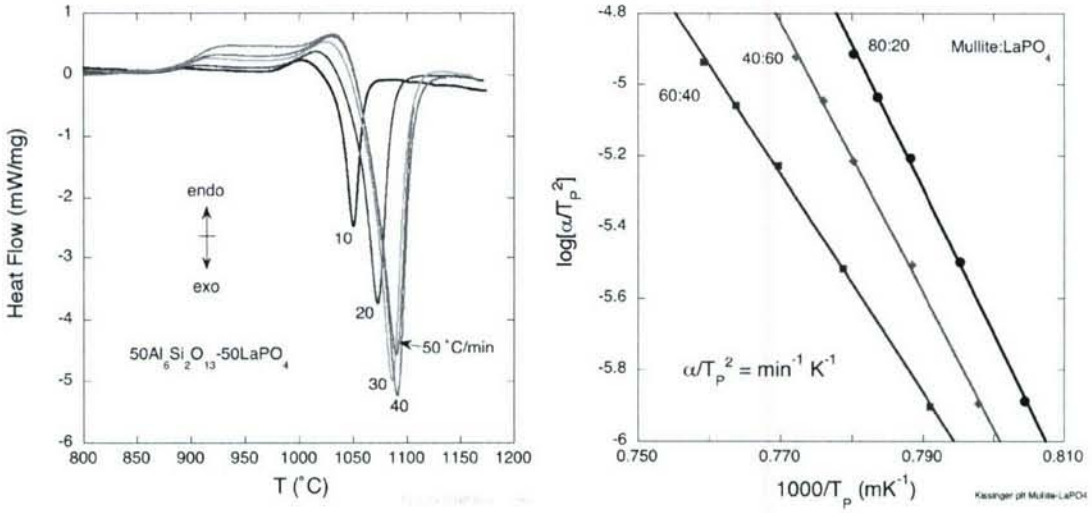

Fig. 10. Nonisothermal crystallization studies on REAPS glasses. Right: A series of DSC thermal traces on $50Al_6Si_2O_{13}$-$50LaPO_4$ glass as a function of heating rate. The shift in glass transition and crystallization temperatures provides information on the crystallization dynamics. Left: Kinsinger plots for different glass compositions. Slopes yield activation energies for nonisothermal crystallization.

Crystallization dynamics. Having identified appropriate compositions for further study, we explored the crystallization dynamics and related crystalline morphologies using different DSC and microscopic techniques. The results provide significant encouragement that glass precursors possess the necessary synthetic functionality to lead to the microstructures needed for ceramic matrix composites. That is, solid state sintering can proceed unhindered by crystallization, and the latter has considerable experimental latitude. Our first extensive study on nucleation and growth in REAPS

glasses was based first on nonisothermal crystallization studies followed by a evaluations of the time-temperature-transformation thresholds as a function of temperature.

Figure 10 (left) shows a series of thermal traces of a 50:50 $Al_6Si_2O_{13}$:$LaPO_4$ (50M50L) glass heated at different heating rates. Certain features of the glass transition and crystallization behavior are seen to shift systematically to higher temperatures. The activation energy of crystallization can be analyzed using the same DSC data. This is presented in Fig. 10 (right) using the Kinsinger[23,32,33] method of analysis. The Kissinger equation assumes an Arrhenian relationship between α/T_P^2 versus $1/T_P$, where α is the thermal ramp rate and T_P is the peak temperature. Figure 10 (right) plots this relationship for selected compositions.

The activation energies for the onset of crystallization are plotted in Fig. 11 (left) as a function of composition. At first sight, the activation energies look quite large, being between 580 and 780 kJ/mol, with respect to many other kinetic phenomena, however, these values are in keeping with nucleation/growth behavior seen in other metal and compound systems. A comparison is made to that measured for mullite glass, which is seen to possess an even higher activation energy of about 892 kJ/mol[23].

At low mullite contents (< 40%), crystalline $LaPO_4$ and mullite nucleate independently at different temperatures, usually first as metastable phases that later

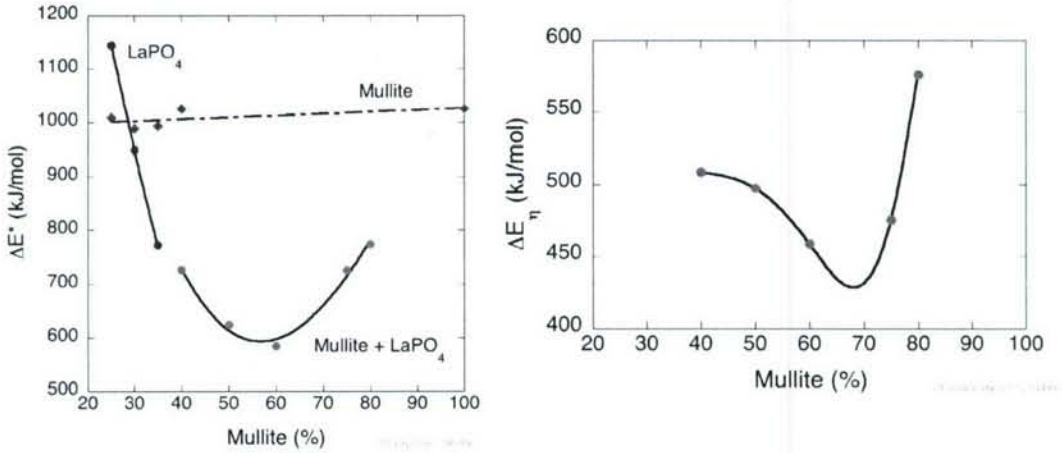

Fig. 11. Activation energies as a function of composition of REAPS glasses between the compositions of mullite and monazite (i.e., $Al_6Si_2O_{13}$ and $LaPO_4$). Left: Activation energies for nonisothermal crystallization. Right: Activation energy for viscous flow as derived DSC scans through the glass transition region.

convert to thermodynamically stable phases at higher temperatures. In the intermediate composition range (40 to 80 % mullite), nucleation and growth of both phases happen simultaneously and cooperatively. This is reflected in Fig. 6 (right) as concurrent nucleation and corresponds to the highest temperatures for crystallization. It is interesting that the greatest spread between the glass transition and crystallization temperatures coincides with the lowest activation energies for crystallization. This indicates that the entropy of crystallization is rather high, consistent with the cooperative

diffusion necessary to separate out components in the glass phase before they nucleate into the two different crystal systems.

Another interesting feature of Fig. 11 (left) is that the activation energy for independent nucleation of mullite at low mullite contents is nearly the same as for pure mullite. This suggests that the entropic effects of amorphous phase segregation does not hinder nucleation and growth mullite in the extreme composition ranges.

Figure 11 (right) presents the activation energies for viscous flow[1]. Like crystallization, viscous flow has the lowest activation energies for intermediate compositions. At first, this seems counterintuitive suggesting that lower activation energies should reflect easier nucleation. On the other hand, there is a thermodynamic driving force for the glass to first separate while in the glassy phase before subsequent crystallization. This emphasizes the role of entropic changes in the process.

Further interpretation of the activation energies derived from nonisothermal studies is complex, because of the combination of several contributions. For single component systems, this will include combined contributions of the energetics of nucleation and molecular transport. In our case, these also include the energetics of amorphous phase segregation, which in turn will depend very much on the separate contributions of interfacial energies and interdiffusion/demixing phenomena. It is our observation that the minimum activation energy corresponds not only with the glass composition of highest crystallization temperature, but also to where the effect of amorphous phase segregation is greatest.

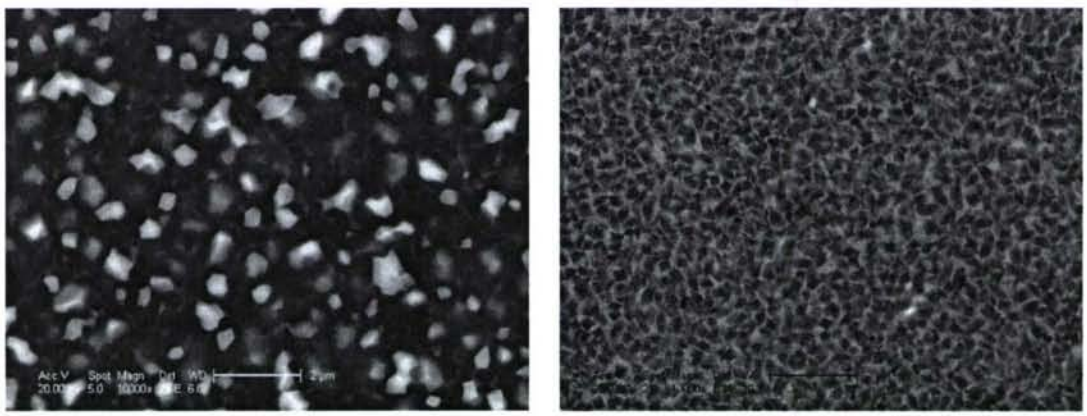

Fig. 12. Comparison of microstructures for different crystallization anneals for glass 60M40L (60% $Al_6Si_2O_{13}$ - 40% $LaPO_4$). **Left**: Higher temperature anneal consists of monazite grains (bright) embedded in mullite matrix. Mullite (dark phase) with monazite precipitates. **Right**: Lower temperature anneal consists of mullite grains and monazite as continuous boundary phase. The magnification is the same in both micrographs.

Crystallization morphologies. The range of morphologies that can be obtained from simple isothermal annealing is illustrated in Fig. 12. Both micrographs correspond to the nominal glass composition of 60% $Al_6Si_2O_{13}$ – 40% $LaPO_4$ on a molar basis. This composition corresponds to a relative volume of 22 v/o of the monazite phase. The glass

annealed at high temperature, 1400°C, yielded discrete precipitates of $LaPO_4$ monazite (bright phase) surrounded in a continuous matrix of a mullite aluminosilicate (black phase).

The opposite observation is made with microstructures in Fig. 12 (right). It is analogous to the microstructure shown in Fig. 1 but with features that are nearly 1/50th of the size. This is interpreted as a case where the mullite crystallizes first, rejecting the lanthanum phosphate at the growth interface and leaving monazite to form at the interfacial boundaries. The mullite grains are on the order of 0.2 μm whereas the La-monazite boundary phase is about 40 nm thick. This structure is not columnar like the melt derived microstructure, but is instead of uniformly distributed, equiaxed grains. The annealing procedure for producing this microstructure was highly fortuitous. While the results are reproducible, the details of leading to the nucleation and growth of the mullite grains and the production of the monazite boundary layer is not understood at all.

This is an important result for producing crystalline composites. Most current design schemes for CMC's places the monazite phase at either phase boundaries or as the matrix[5,34-37]. The fact that crystallization can be manipulated with a high degree of flexibility suggests that it will be possible to use directional crystallization techniques to add orientational biases to the fracture behavior of composites. Proving this is one of our goals.

In contrast to this example, other much less desirable microstructures are derived from alternative thermal histories. The difference is likely due to relaxation processes occurring in the glass phase at the early stages before and during nucleation. The processes involved are complex, sometimes appearing contradictory, but nevertheless are a result of the complex chemistry of the glass structure. This illustrates the need to conduct detailed and comprehensive fundamental investigations of the glass structure and the dynamical mechanisms of mass transport leading to the nucleation growth of the two crystalline phases. It is evident that there is a hierarchy of overlapping and cooperative mechanisms involved.

Densification via Viscous Sintering. An important practical objective of this project was to investigate the feasibility of sintering glass powders in the glassy state and then crystallize monolithic glass part in a separate step. We conducted a brief study on the 50M50L composition to prove that it is indeed will be possible. Figure 13 present a collage of figures that demonstrates this point.

First a time-temperature-transformation (TTT) diagram was first constructed from isothermal crystallization experiments conducted by temporal differential scanning calorimetry. Figure 13 (upper left) shows a schematic of the heat exchange as a function of time during isothermal anneals for different temperatures. Crystallization is shown as an exothermic peaks. At high temperatures, the onset and completion of crystallization is rather quick, where the exothermic peak is relatively sharp and narrow with respect to time. At lower temperatures, the onset of crystallization is slower, occurring later in the anneal, and the exothermic peaks are relatively broader and shallower. Figure 13 (lower left) summarizes the onset and completion of crystallization as measured by these DSC traces. The results are typical of nucleation phenomena, indicating that crystallization is slower and more sluggish at lower temperatures.

One densification experiment was also conducted at 940°C on the 50M50L glass composition composition. This temperature was above the glass transition temperature (875°C) and the nonisothermal crystallization temperature (1062°C) shown in Fig. 6 for the same composition. Figure 13 (upper right) plots the density of the glass powder compact as a function of time up to about 55 minutes of annealing. The powder compact reached a density of 93% of theoretical. A check on the TTT diagram indicates that the onset of crystallization should not occur until after about 180 minutes of annealing at this temperature. Indeed, x-ray diffraction did not indicate any crystallization at this time. Consequently, densification took place by viscous sintering. This is desirable since viscous sintering is inherently faster than if crystalline phases are present at this temperature. It is worth noting here that this experiment made no special effort to optimize the power size in order to increase the rate of sintering. The initial powders were classified by a 325 mesh (less than 15 microns) and does not represent the state of what is possible by modern sintering technology. The expectation is therefore that it will indeed be possible to sinter glass powders to high density without the interference of premature crystallization. Subsequent to this, it should be possible to carry out a separate nucleation and growth step under various different schemes to produce directionally oriented microstructures.

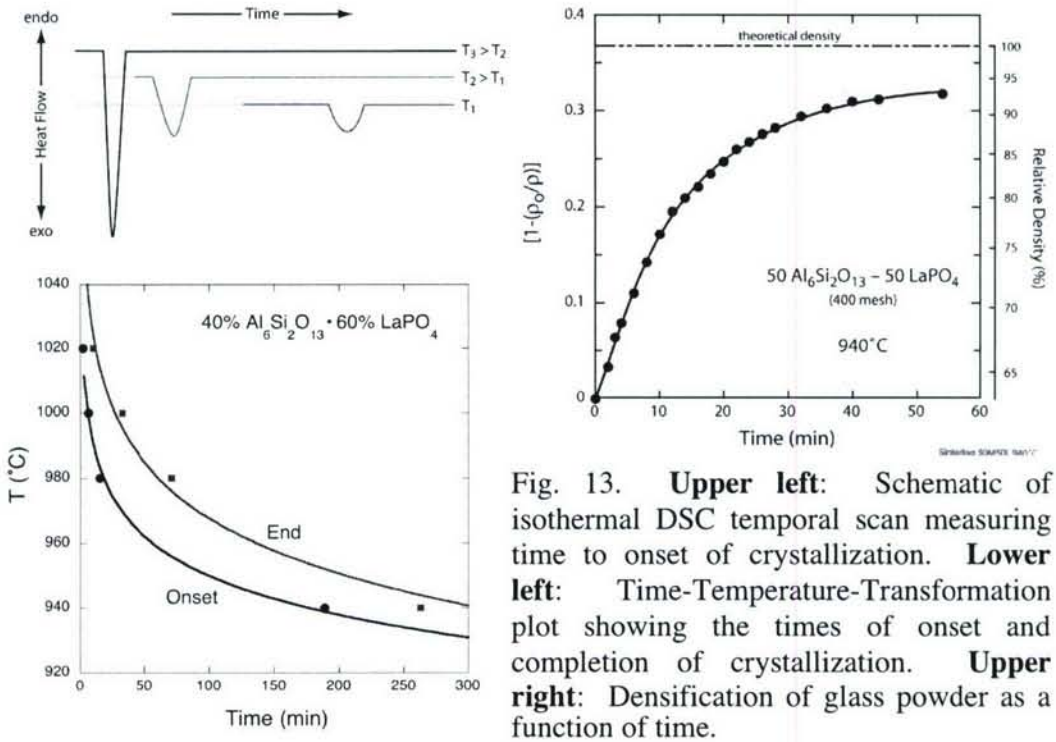

Fig. 13. **Upper left**: Schematic of isothermal DSC temporal scan measuring time to onset of crystallization. **Lower left**: Time-Temperature-Transformation plot showing the times of onset and completion of crystallization. **Upper right**: Densification of glass powder as a function of time.

<u>*Sol-gel synthesis vs. thermally quenched glasses*</u>. The fundamental studies carried out on this system, thus far, has been based on quenched melt glasses. Our synthetic method typically yields about 0.5 to 5.0 grams of material for each run which is not much since we are now interested in larger pieces for experimentation. While quench process can be scaled up, it is desirable to test other production methods that could yield much larger

quantities of glass with less effort. It is also desirable to develop methods that will produce glass powders directly rather than crushing glass beads of quenched glass. We have been exploring and developing an aqueous sol gel chemistry based upon polyacrylamide gelation. Our process is a modification of a successful procedure already designed for oxides related to our system, namely, mullite and $LaAlO_3$[38,39], to include phosphates. A rather successful comparison can be made to the quality of the quenched glasses.

Figure 14 compares a sequence of ^{27}Al MAS NMR spectra of a glass of final composition of $xAl_2O_3 \bullet (1\text{-}x)AlPO_4$ ($x = 0.5$) after annealing at different temperatures. Both x-ray diffraction and thermal analysis show that the organics are effectively driven off above 600°C. Moreover, crystallization for sol gel derived glasses occurs at 1050°C, which is nearly identical as that for thermally quenched glasses.

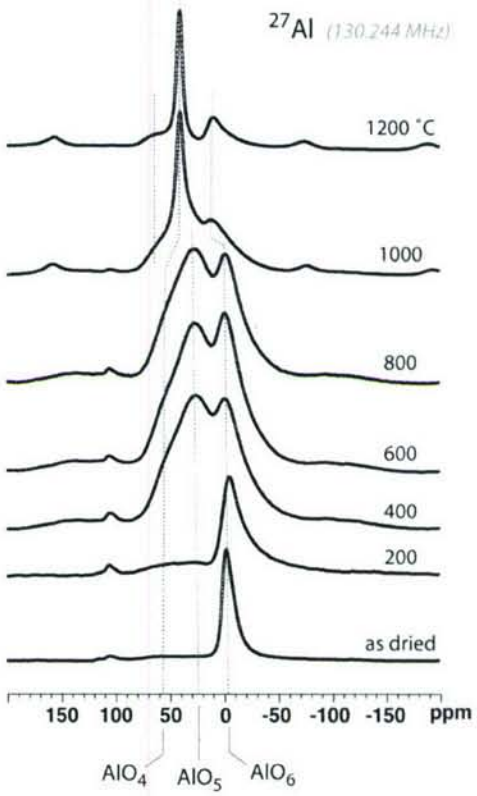

Fig. 14. ^{27}Al MAS NMR spectra of $xAl_2O_3 \bullet (1\text{-}x)AlPO_4$ ($x = 0.5$) sol gel glasses annealed at different temperatures. Crystallization occurs between 800 and 1000 °C.

This result encourages us to expand the chemistry to include rare earths and silica. An addition advantage is the all of the hydrocarbons are burned off by 600°C with almost no residual carbon. This will avoid the problem of carbothermal reduction of phosphorous that has been observed for such compounds as $LaPO_4$ via another other sol gel route[40]. Based upon this result, we feel that there is advantage in future research to develop sol-gel methods for synthesizing large scale batches of REAPS glass powders which subsequently can be used for viscous sintering and the conversion to CMC's.

Project Participants

Personnel Supported by Grant

Significant support

Shuling Guo	Ph.D., Science & Engineering of Materials, ASU-Tempe
Swati Gupta	M.S., Science & Engineering of Materials, ASU-Tempe

Partial support

Feng He	Graduate Student, School of Materials, ASU-Tempe
Linda Stearn	Graduate Student, Chemistry & Biochemistry ASU-Tempe
William T. Petuskey	Professor (P.I.), Arizona State University, Tempe, AZ

Other Participants

Paul F. McMillan	Dept. of Chemistry, University College London, UK
Masahiro Yoshimura	Dept. of Materials Engineering, Tokyo Institute of Technology

Project Activities: List of Reports and Presentations

Publications:

"Melt structure in the Al_2O_3-CaO-$LaPO_4$ system studied by Raman scattering and ultra high-temperature ^{27}Al NMR," J. Piwowarczyk, R.F. Marzke, B.H. Takulapalli, G.H. Wolf, P.F. McMillan and W.T. Petuskey, J. Eur. Ceram. Soc., 25 [8] 1333-1340 (2005).

"Synthesis and Characterization of Al_2O_3–P_2O_5 Glasses Derived by a Sol-Gel Method," Swati Gupta, M.S. Thesis, Science and Engineering of Materials, Arizona State University, August 2006.

"Glass Formation and Crystallization in the Alumina-Silica-Lanthanum Phosphate System for Ceramics Composites," Shuling Guo, Ph.D. dissertation, Science and Engineering of Materials, Arizona State University, December 2006.

Written reports:

Interim Report #1, "High Temperature Liquid and Glass Precursors for Oxyphosphate Ceramic Composites", for the period 4/1/04 to 8/31/04, submitted for the AFOSR 2004 Contractors Meeting, Ceramic and Non-Metallic Materials, Wintergreen, VA, August 16-18, 2004

Interim Report #2, "High Temperature Liquid and Glass Precursors for Oxyphosphate Ceramic Composites", for the period 9/1/04 to 8/31/05, submitted for the AFOSR 2005 Aerospace and Materials Science Programs Review 2005; Sedona, Arizona, August 15-17, 2005

Interim Report #3, "High Temperature Liquid and Glass Precursors for Oxyphosphate Ceramic Composites", for the period 9/1/04 to 9/30/05, submitted

for the AFOSR 2006 Ceramics Program Review, Washington, DC, Workshop, Arlington, VA, November 1-2, 2006.

Oral Presentations:

"High Temperature Liquid and Glass Precursors for Oxide-Phosphate Ceramic Composites," W. T. Petuskey, AFOSR 1004 Contractors Meeting, Ceramic and Non-Metallic Materials, Wintergreen, VA, August 16-18, 2004

"Molten and Glass Phase Precursors for Oxide-Phosphate Composites," William T. Petuskey and Shuling Guo, Invited Presentation, Conference on Composites at Lake Louise; Lake Louise, Alberta, Canada, November , 2005

"High Temperature Liquid and Glass Precursors for Oxyphosphate Ceramic Composites," William T. Petuskey, Invited presentation, AFOSR Aerospace and Materials Science Programs Review 2005; Sedona, Arizona, August 15-17, 2005

"Issues of Chemistry on Designing Ceramics for Mechanical Applications," W. T. Petuskey, Workshop on the "Synthesis, Design and Function in New Materials Chemistry", Meeting of the Portfolio Partnership Collaboration with the Solid State Group of Royal Society, Invited Presentation, University College of London, UK, March 28-30, 2006

"Synthesis and Structural Analysis of Glasses and Glass Ceramics in the CaO-Al_2O_3-$LaPO_4$ System," R. F. Marzke, S. C. Boucher, J. Piwowarczyk, G. Wolf, W. Petuskey, 8th International Symposium on Crystallization in Glasses and Liquids, Jackson Hole, Wyoming, September 24-28, 2006.

"Molten and Glass Phase Precursors for Rare Earth Aluminophosphosilicate Composites (REAPS)," W. T. Petuskey, S. Guo, S. Gupta, F. He, P. F. McMillan, 8th International Symposium on Crystallization in Glasses and Liquids, Jackson Hole, Wyoming, September 24-28, 2006.

"High Temperature Liquid and Glass Precursors for Oxide-Phosphate Ceramic Composites," W. T. Petuskey, AFOSR Ceramics Program Review, Washington, DC, Invited, Workshop, Arlington, VA, November 1-2, 2006.

"REAPS Glasses and Glass-Ceramics," W. T. Petuskey, Naming Ceremony of the LeRoy Eyring Center for Solid State Science Colloquium, Tempe, Arizona, March 23, 2007

References

(1) Guo, S. Ph.D., Arizona State University, 2006.

(2) Pai, D. M.; Yarmolenko, S.; Sankar, J.; Kailasshankar, B.; Murphy, C.; Freeman, E.; Zawada, L. P. *Materials Research Society Symposium Proceedings* **2004**, *795*, 429-434.

(3) Mawdsley, J. R.; Kovar, D.; Halloran, J. W. *Journal of the American Ceramic Society* **2000**, *83*, 802-808.

(4) Morgan, P. E. D.; Marshall, D. B. *Materials Science and Engineering* **1993**, *A162*, 15-25.

(5) Morgan, P. E. D.; Marshall, D. B. *J. Am. Ceram. Soc.* **1995**, *78*, 1153-56.

(6) Morgan, P. E. D.; Marshall, D. B.; Davis, J. B.; Housley, R. M. 1999, p 229-243.

(7) Brow, R. K.; Wittenauer, A. K. *Phosphorus Research Bulletin* **2002**, *13*, 95-100.

(8) Karabulut, M.; Metwalli, E.; Brow, R. K. *J. Non-Cryst. Sols* **2001**, *283*, 211-219.

(9) Karabulut, M.; Metwalli, E.; Wittenauer, A. K.; Brow, R. K.; Marasinghe, G. K.; Booth, C. H.; Bucher, J. J.; Shuh, D. K. *Journal of Non-Crystalline Solids* **2005**, *351*, 795-801.

(10) Rosenflanz, A.; Frey, M.; Endres, B.; Anderson, T.; Richards, E.; Schardt, C. *Nature (London, United Kingdom)* **2004**, *430*, 761-764.(11)James, P. F. *Journal of Materials Science* **1975**, *10*, 1802-25.

(12) Mao, H.; Selleby, M.; Sundman, B. *Journal of the American Ceramic Society* **2005**, *88*, 2544-2551.

(13) Bonneau, C.; McMillan, P. F. 2001, p 867-868.

(14) McMillan, P. *Nature (London)* **2000**, *403*, 151-152.

(15) McMillan, P. F. 1998, p 2135-2139.

(16) McMillan, P. F.; Ho, C.; Aasland, S.; Yeganeh-Haeri, A.; Weber, R. *Materials Research Society Symposium Proceedings* **1997**, *455*, 377-379.

(17) Wilding, M. C.; McMillan, P. F.; Navrotsky, A. *Physica A: Statistical Mechanics and Its Applications (Amsterdam, Netherlands)* **2002**, *314*, 379-390.

(18) Angell, C. A. *Science (Washington, D. C.)* **1995**, *267*, 1924-35.

(19) Moynihan, C. T. *Journal of the American Ceramic Society* **1993**, *76*, 1081-7.

(20) Moynihan, C. T.; Lee, S. K.; Tatsumisago, M.; Minami, T. *Thermochimica Acta* **1996**, *280/281*, 153-162.

(21) Brow, R. K.; Metwalli, E.; Sidebottom, D. L. *Proceedings of SPIE-The International Society for Optical Engineering* **2000**, *4102*, 88-94.

(22) Johnson, B. R., 2001.

(23) Johnson, B. R.; Kriven, W. M.; Schneider, J. *Journal of the European Ceramic Society* **2001**, *21*, 2541-2562.

(24) Boucher, S.; Piwowarczyk, J.; Marzke, R. F.; Takulapalli, B.; Wolf, G. H.; McMillan, P. F.; Petuskey, W. T. *Journal of the European Ceramic Society* **2005**, *25*, 1333-1340.

(25) He, H.; Guo, J.; Zhu, J.; Yuan, P.; Hu, C. *Spectrochimica Acta, Part A: Molecular and Biomolecular Spectroscopy* **2004**, *60A*, 1061-1064.

(26) He, H. P.; Guo, J. G.; Zhu, J. X.; Hu, C. *Clay Minerals* **2003**, *38*, 551-559.

(27) McManus, J.; Ashbrook, S. E.; MacKenzie, K. J. D.; Wimperis, S. *Journal of Non-Crystalline Solids* **2001**, *282*, 278-290.

(28) Schmuecker, M.; Schneider, H.; MacKenzie, K. J. D.; Smith, M. E.; Carroll, D. L. *Journal of the American Ceramic Society* **2005**, *88*, 2935-2937.
(29) Hartmann, P.; Jana, C.; Vogel, J.; Jaeger, C. *Chemical Physics Letters* **1996**, *258*, 107-112.
(30) Kentgens, A. P. M.; Bos, A.; Dirken, P. J. *Solid State Nuclear Magnetic Resonance* **1994**, *3*, 315-22.
(31) Woo, A. J. *Bulletin of the Korean Chemical Society* **1999**, *20*, 1205-1208.
(32) Kissinger, H. E. *J. Research Natl. Bur. Standards* **1956**, *57*, 217-21.
(33) Yinnon, H.; Uhlmann, D. R. *Journal of Non-Crystalline Solids* **1983**, *54*, 253-75.
(34) Boakye, E. E.; Petry, M. D.; Hay, R. S. In *U.S.*; (United States Dept. of the Air Force, USA). US, 1998, p 3 pp.
(35) Chawla, K. K.; Liu, H.; Janczak-Rusch, J.; Sambasivan, S. *Journal of the European Ceramic Society* **2000**, *20*, 551-559.
(36) Davis, J. B.; Marshall, D. B.; Morgan, P. E. D. *Journal of the European Ceramic Society* **2000**, *20*, 583-587.
(37) Keller, K. A.; Parthasarathy, T. A.; Mah, T.-I.; Cinibulk, M. K.; Boakye, E. E. *Ceramic Engineering and Science Proceedings* **1999**, *20*, 451-461.
(38) Douy, A. *Journal of the European Ceramic Society* **1991**, *7*, 117-23.
(39) Douy, A.; Odier, P. *Materials Research Bulletin* **1989**, *24*, 1119-26.
(40) Mawdsley, J. R.; Halloran, J. W. *Journal of the European Ceramic Society* **2001**, *21*, 751-757.